Supplementary Information: Control of superselectivity by crowding in three-dimensional hosts

Andrew T. R. Christy
Department of Chemistry, Durham University, South Road, Durham, DH1 3LE, United Kingdom

Halim Kusumaatmaja*
Department of Physics, Durham University, South Road, Durham, DH1 3LE, United Kingdom

Mark A. Miller†
Department of Chemistry, Durham University, South Road, Durham, DH1 3LE, United Kingdom

Appendix A: Further Simulation Details

In this work, two types of binding model are employed to describe two common interactions observed within membraneless organelles: isotropic binding (representing generic non-specific attraction) and directional binding (representing binding at mutually specific sites on the two species) [1]. In general, the interaction energy between two beads, i and j, is given by:

$$E_{ij} = \delta_{ij}\varepsilon_{ij}, \tag{A.1}$$

where ε_{ij} is the interaction strength between beads i and j. For a client–receptor pair, ε_{ij} takes the value $-f$, with $f > 0$ corresponding to attractive interactions. For other combinations of bead types, $\varepsilon_{ij} = 0$. The Kronecker delta δ_{ij} determines whether or not the two beads are bound. When isotropic bonds are activated, all beads on adjacent lattice sites are automatically bound, and therefore δ_{ij} is 1 for all adjacent beads and 0 for any pair of beads separated by more than one step on the lattice. In contrast, when directional bonding is applied, each bead can only form one bond. Thus, the calculation of δ_{ij} requires MC moves for bond breaking and bond formation. The bond formation move involves randomly selecting a client bead neighboring a receptor and attempting a bond formation with an acceptance probability of

$$P^{\mathrm{acc}} = \min\left[1, \omega e^{-\Delta E/kT}\right]. \tag{A.2}$$

ΔE is the change in energy of the move. The weighting factor $\omega = N_{\mathrm{u}}/(N_{\mathrm{b}} + 1)$ is needed to ensure the move obeys detailed balance, where N_{u} and N_{b} are the number of unbound and bound client–receptor pairs, respectively. For the bond-breaking move, we can also use a similar method. However, in this case, client–receptor bonds are selected randomly and the weighting factor in the acceptance probability for the selected bond to be broken becomes $\omega = N_{\mathrm{b}}/(N_{\mathrm{u}} + 1)$ [2].

In the simulations, the client is able to explore the system by reptation, individual bead displacement and teleport moves. In the reptation move, the end bead is deleted and a bead is randomly positioned, within the linker range, at the other end of the chain. Individual bead displacements correspond to moves in which a bead is randomly selected and moved to a new position. Teleport moves involve the deletion of the client and the regrowth from a randomly selected lattice site. This regrowth involves sequentially positioning client beads a random displacement from the previous bead. All these moves are immediately rejected if they result in two beads occupying the same lattice site or the implicit linkers becoming broken. If the move is not limited by either one of these two constraints, it is then accepted with a probability of

$$P^{\mathrm{acc}} = \min\left[1, e^{-\Delta E/kT}\right]. \tag{A.3}$$

As before, ΔE is the change in energy of the trial move [2]. We also note that, in the directional binding case, all chain moves that involve a bond being broken are rejected and no bonds are formed in bead displacement moves, in order to obey detailed balance.

To ensure that the system is fully explored by the client, we typically use 10^8 MC moves for the directional binding case and 5×10^8 for the isotropic binding case. The ability of the client to explore the system fully was monitored

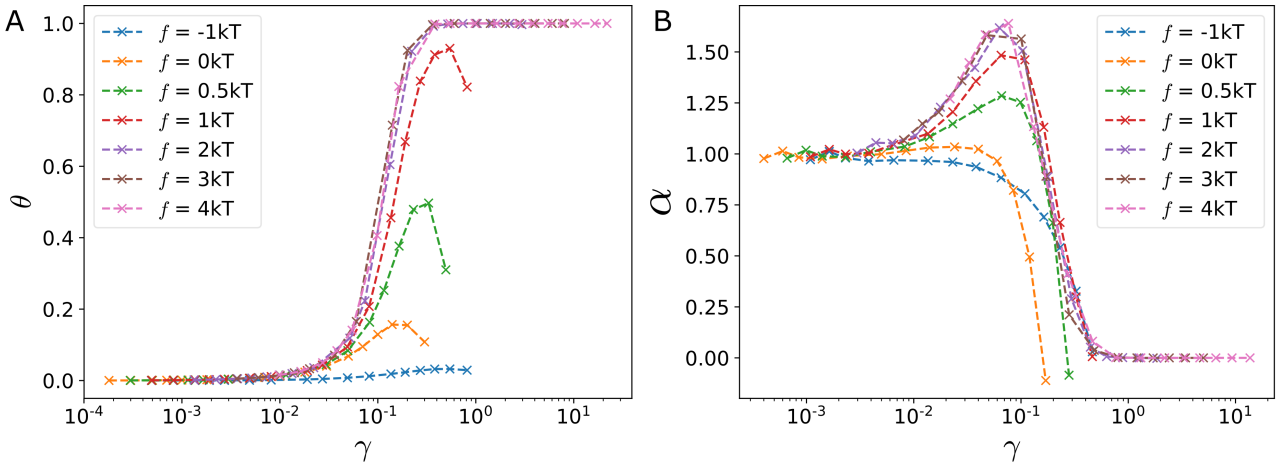

FIG. S1: Simulation results for a decavalent client with linker length $l = 5$ exploring a system of crowders (at density of 0.4) and receptors in the directional binding case, for an interaction strength between the client beads and receptors ranging from $-1kT$ to $4kT$. (A) Client binding probability θ as a function of scaled receptor density γ. (B) Superselectivity parameter $\alpha = d\ln\theta/d\ln n_{\mathrm{R}}$ against scaled receptor density $\gamma = n_{\mathrm{R}}e^{-f/kT}$.

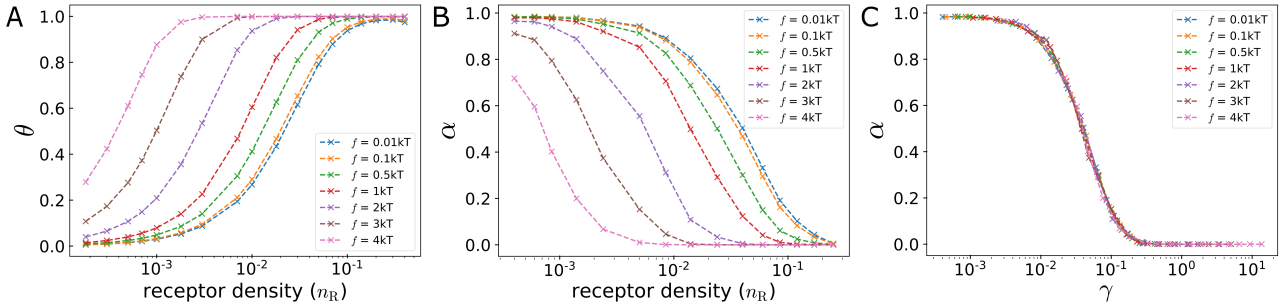

FIG. S2: Simulation results for a decavalent client with linker length $l = 5$ exploring a system of receptors in the absence of crowders. The strength of the directional interaction between the client and receptor beads range from $0.01kT$ to $4kT$. (A) Client binding probability θ as a function of receptor density γ. Superselectivity parameter $\alpha = d\ln\theta/d\ln n_{\mathrm{R}}$ against (B) receptor density n_{R} and (C) scaled receptor density $\gamma = n_{\mathrm{R}}e^{-f/kT}$.

throughout this work, to ensure that the binding occurred all the way through the slab and not predominantly at the interface. Sampling only became an issue when the combined packing fraction of receptors and crowders in the scaffold was 0.8 or greater. In all cases studied, the binding transition had already occurred at lower densities. Therefore the inability of the client to penetrate the scaffold at extremely high densities had no impact on the findings in the paper.

Appendix B: Varying interaction strength and linker length in the directional binding case

In this section we provide additional results for the directional binding case. Here we have set the scaffold to free volume ratio to 1:1. Variation in the volume ratio will be further explored in the next section. Figure S1 shows how superselectivity depends on the interaction strength f for the directional binding case. Increasing the interaction strength lowers the receptor density at which binding starts. This enthalpic effect can be accounted for by plotting the probability θ of binding as a function of the parameter $\gamma = n_{\mathrm{R}}e^{-f/kT}$ [3], where n_{R} is the density of binding beads, defined as the fraction of lattice sites in the scaffold region that the binding beads occupy. As panel (A) of Fig. S1 shows, when plotted in this way, the binding curves overlap for sufficiently strong binding strengths ($f \geq 2kT$).

As the interaction strength weakens below $f = 2kT$, the onset of binding is shifted to higher receptor densities. However, the combination of the crowder beads and the increased number of receptor beads then makes the overall

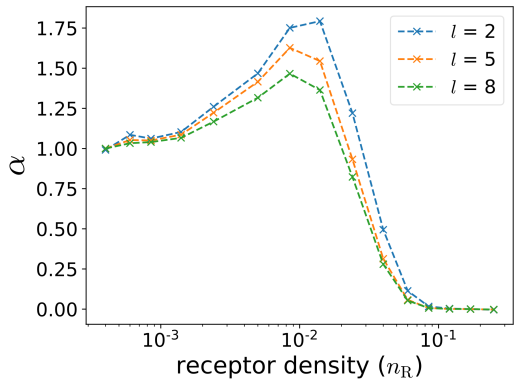

FIG. S3: Simulation results for a single decavalent client, with interaction strength of $2kT$, in a system containing crowders at density 0.4, for several linker lengths

density of the scaffold region very high, thereby increasing the entropic cost for the client to enter the scaffold. Superselectivity is therefore suppressed by the reduced enthalpic gain and higher entropic penalty for multivalent binding. This effect is quantified in Fig. S1(B), which shows the superselectivity parameter $\alpha = d\ln\theta/d\ln n_{\mathrm{R}}$ as a function of the scaled receptor density γ. The peak $\alpha > 1$ is unchanged over a wide range of f but is systematically reduced and eventually eliminated when f becomes too small.

To provide additional evidence on the importance of crowders for superselectivity in 3D, we have also carried out simulations for a wide range of interaction strengths in the absence of crowders, from $f = 0.01kT$ to $4kT$. The results are presented in Fig. S2. When the volumes of the scaffold and free regions are comparable, we never find superselective binding. Lower interaction strengths do shift the binding transition to higher n_{R} values, but this shift does not change the steepness of the binding transition. In fact, the binding curves collapse onto a master curve when the receptor density is rescaled through γ.

We have also studied the impact of varying linker length between the client binding beads. The results are shown in Fig. S3, where it can be seen there is some anti-correlation between superselectivity and the length of the linkers. Recall that the linkers are represented implicitly as a maximum tether length between binding beads [4], so conformations of the linker sections are not captured explicitly. The implicit linker representation also means that the total excluded volume of a client depends only on the valency (the number of binding beads) and not on the linker length. However, for short linkers, the volume-occupying beads are more concentrated in space. Hence, binding of even a single bead to a scaffold receptor site places severe constraints on the conformation that the whole client may adopt.

Appendix C: Varying the free volume

The majority of results in this article are for a scaffold system adjacent to an empty cytosol region of equal volume. However, as we have seen in the main text, superselectivity can be observed in the absence of crowders at sufficiently large volume ratio between the free space and the scaffold.

To probe the entropic origins of this effect, we return to our analysis of multivalent client binding compared to that of monovalent clients. Here, we use a system of scaffold to free volume ratio of 1:10, and study the binding behaviour without and with crowders as a function of the receptor density. The results are shown in Fig. S4(A) and Fig. S4(B), respectively. In both cases, a signature of superselective binding is the compression of the binding response into a narrower range of receptor density, due to a suppression at low receptor density and an increase of binding probability at high receptor density. Comparing Fig. S4(A) and Fig. S4(B), we can further conclude that this effect is much stronger in the case with crowders.

Our direct computer simulations have a practical limitation on the ratio of free space to scaffold volume of $O(1000)$. To demonstrate the dominant effect of crowders in superselective binding for even larger volume ratio, we use a statistical mechanical argument to extrapolate from the binding curve measured in simulations at a computationally accessible volume ratio. First, we split the partition function of the client molecule into three terms:

$$Q = Q_{\mathrm{b}} + Q_{\mathrm{ref}} + (V - V_{\mathrm{ref}})Q_{\mathrm{u}}. \tag{A.4}$$

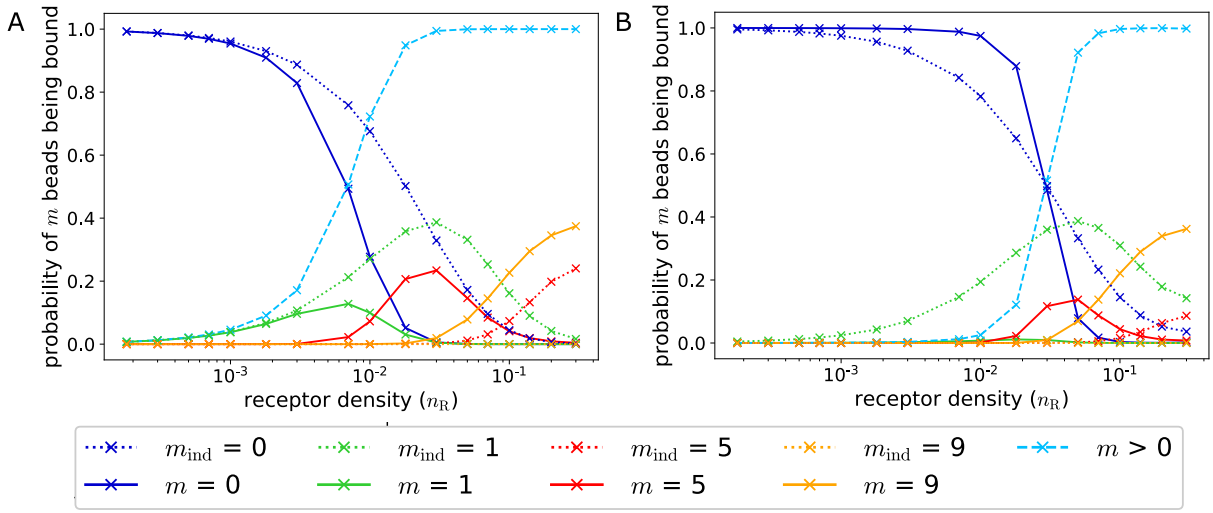

FIG. S4: Probability of m beads being bound in a system of parameters $l = 5$, $f = 2kT$ and with scaffold to free volume ratio of 1:10. The dashed lines are for ten monovalent clients and the solid lines are for a single decavalent client. These plots are for systems (A) without crowders and (B) with crowders at density $d = 0.4$.

Here, Q_b, the partition function for bound configurations in the scaffold and Q_{ref} is the partition function of unbound configurations for a reference volume V_{ref} of free space. Both these contributions are affected by the presence of the scaffold, since steric interactions between the client and the scaffold will restrict the conformations that the client can adopt, even if the client is not bound to the scaffold. The only requirement on V_{ref} is that it is large enough to include all unbound conformations of the client that do involve steric interactions with the scaffold. Finally, Q_u is the partition function per unit volume of unbound configurations in the bulk cytosol, far away from any interfaces. This term captures the internal configurations of the client for a fixed center of mass. Given this decomposition of Q, the probability of binding is

$$P_b = \frac{Q_b}{Q_b + Q_{ref} + (V - V_{ref})Q_u}. \tag{A.5}$$

The contributions Q_b and Q_{ref} do not depend on the actual volume V of the system, while the free-volume term scales linearly with the volume. Eq. (A.5) can be rearranged to give

$$\frac{1}{P_b} = 1 + \frac{Q_{ref}}{Q_b} + (V - V_{ref})\frac{Q_u}{Q_b}. \tag{A.6}$$

Fitting $1/P_b$ a function of V from available simulation data at a given receptor density, we can readily infer the values of $(1 + Q_{ref}Q_b^{-1} - V_{ref}Q_uQ_b^{-1})$ and $Q_uQ_b^{-1}$ for that receptor density. This, in turn allows us to extrapolate a point on a binding curve to arbitrarily large volume ratio without carrying out prohibitively expensive simulations. Repeating the process for each receptor density in a binding curve allows the entire curve to be mapped to a different volume ratio, as shown in Fig. S5 for ratios up to 1:10000. The perfect agreement of the explicit simulations and extrapolated predictions for volume ratios 1:50 and 1:1000 demonstrate the reliability of the calculation. Importantly, the effect of the crowders remains pronounced and continues to enhance superselectivity even in the limit of large volume ratio between the free space and the scaffold domain.

Appendix D: Simulations with multiple clients

Throughout this paper, we have presented results using only a single client. Here we demonstrate that these results are representative of the dilute regime in which the clients are at significantly lower concentrations than the scaffold, as has been studied experimentally by Banani et al. [5] and Jo and Jung [6], among others. Typically, the client concentrations are several orders of magnitude lower than the scaffold concentrations.

Fig. S6 compares the simulation results using 1 and 50 decavalent clients for the directional binding case, corresponding to a client volume fraction of $\phi = 8 \times 10^{-5}$ and $\phi = 4 \times 10^{-3}$ respectively. The fraction of bound clients

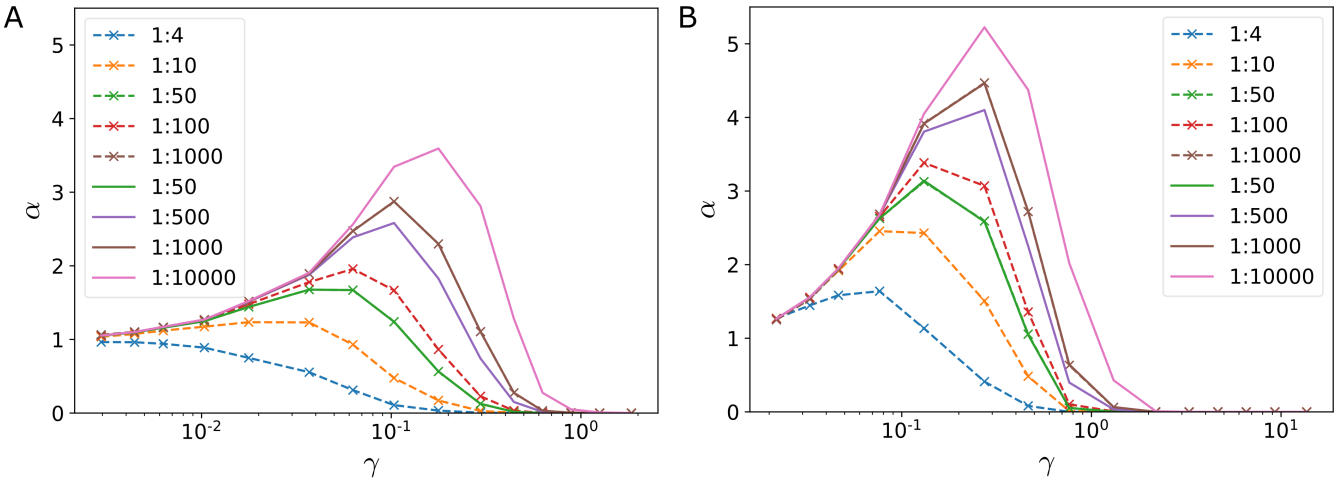

FIG. S5: Superselectivity parameter α for a single client in simulation systems with various ratios of scaffold volume to free space, for a scaffold (A) without and (B) with crowders at density $d = 0.4$. Dashed lines are simulation results, and solid lines are predicted curves from Eq. A.6. The clients were decavalent with linker length $l = 5$ and interaction strength of $f = 2kT$.

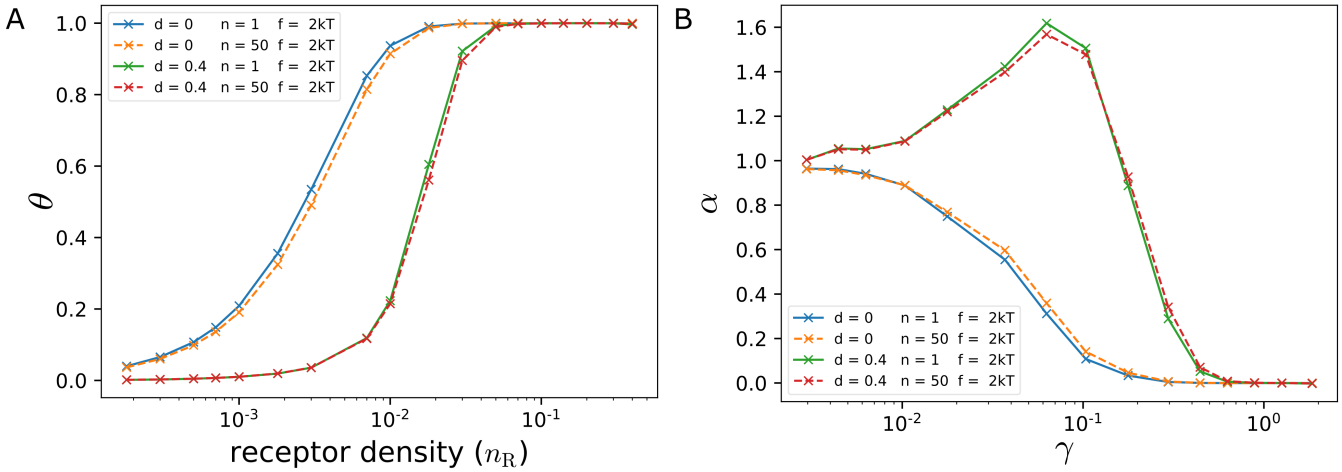

FIG. S6: Results for simulations of 50 clients within the system, where (A) shows the probability of binding at various receptor densities and (B) shows the variation in α with γ.

and the superselectivity behaviour observed are essentially identical. We only start seeing significant deviation for 100 clients, corresponding to a client fraction of $\phi = 8 \times 10^{-3}$.

The structure and composition of membranelles organelles remain a very active area of research, and the proportions of client and scaffold molecules that form stable droplets depend strongly on the types of membranelles organelles [7, 8]. We expect higher client concentrations to alter the scaffold structure [9], and this is an interesting and important area for future work.

Appendix E: Isotropic binding

The results for the isotropic binding case align well with those of the directional binding case, as can be seen in Fig. S7. We observe that superselectivity increases with increasing crowder density and client valency in panels (A) and (B), respectively. However, deviations from the directional binding case can be observed for variations in linker length and binding strength, as illustrated in panels (C) and (D). The key new effect for isotropic binding is due to

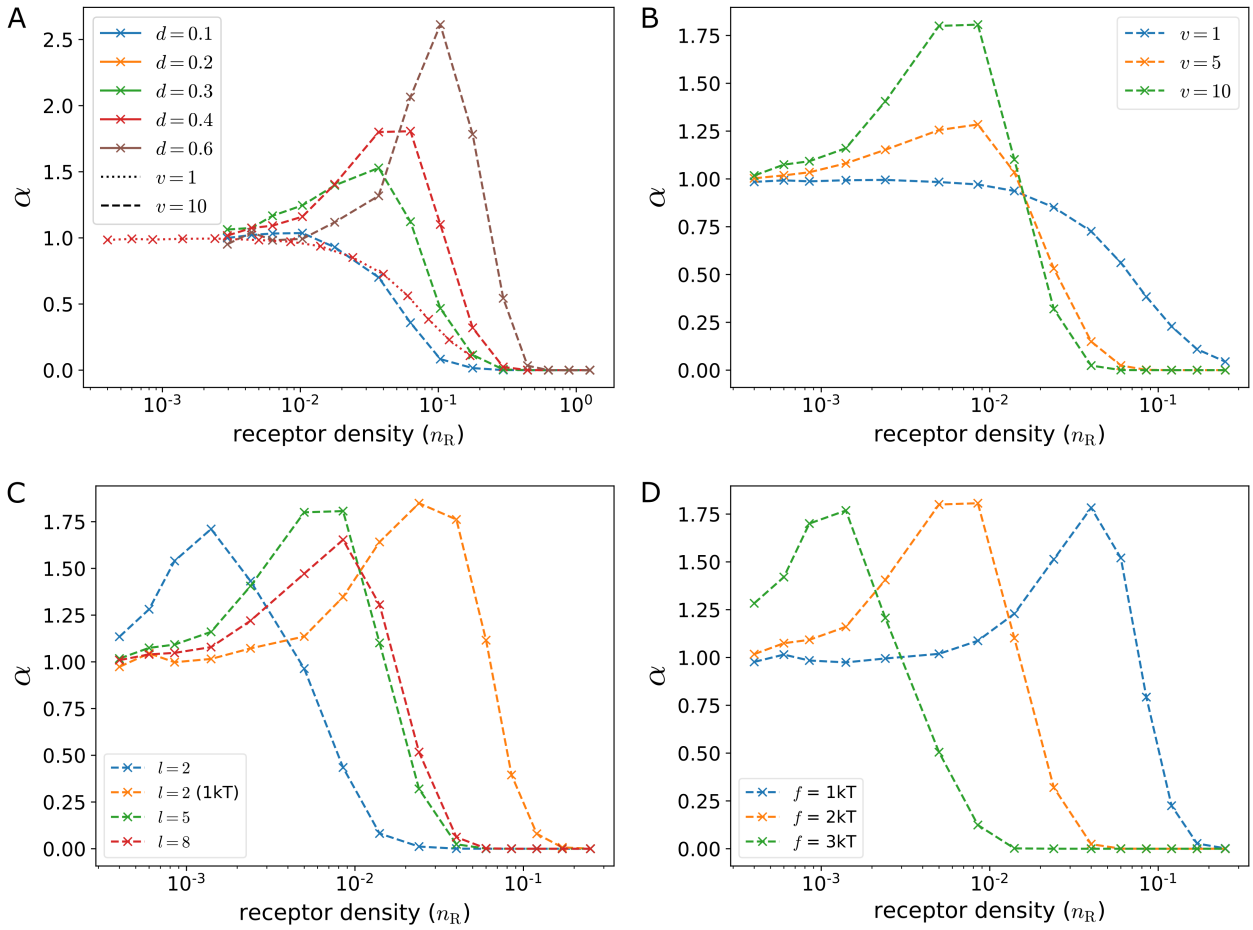

FIG. S7: The superselectivity parameter α as a function of n_R for a variety of parameters: (A) the density d of crowders in the receptor slab, (B) the valency of the client v, (C) the linker length of the client l, and (D) the interaction strength between the client and receptors f. In each of these plots the variables are $v = 10$, $l = 5$, $f = 2kT$ and $d = 0.4$, unless stated otherwise. All results in this figure are for the case of isotropic binding.

the possibility of forming bonds between multiple beads of the client and a single receptor bead, which is not allowed in the directional model.

By forming multiple bonds, the effective density of receptor sites is increased and the client can more easily overcome the entropic cost of entering the 3D host. An extreme case is shown in Fig. S7(C) for $l = 2$, where the receptor beads are surrounded by a client, resulting in the peak in α at very low n_R. Such behavior requires the client to adopt a compact structure. Correspondingly, as further shown in Fig. S7(C), we can delay the peak in α by increasing the entropic barrier by using longer linker length, or by decreasing the enthalpic gain by employing weaker interaction strength (comparing $f = 2\,kT$ and $f = 1\,kT$ for $l = 2$).

Similar behavior is also observed in Fig. S7(D) for $l = 5$ when we vary f from $1\,kT$ to $3\,kT$. These shifts in n_R values for the peaks of α differentiate the isotropic from the directional binding case. For the latter, the shifts are not observed upon variation in linker length. The shifts for variations in interaction strength also cannot be captured by the parameter γ introduced in the previous section. In fact, since the client can form multiple bonds, the use of γ instead of θ for the binding probability plots is generally not helpful.

Figure S8 shows the probability of m beads being bound for the isotropic binding case, in systems both with and without crowders. As with the directional binding case, the probability of one bead being bound is greatly suppressed for a multivalent client compared to monomers in a system with crowders, but not when crowders are absent. The main difference between the directional and isotropic binding cases is that the cooperative effect sets in at lower n_R. This can be seen by comparing the lines corresponding to 5 beads being bound, for the decavalent and monovalent clients. This is likely a result of the client being able to form many more bonds in the isotropic binding case, compared

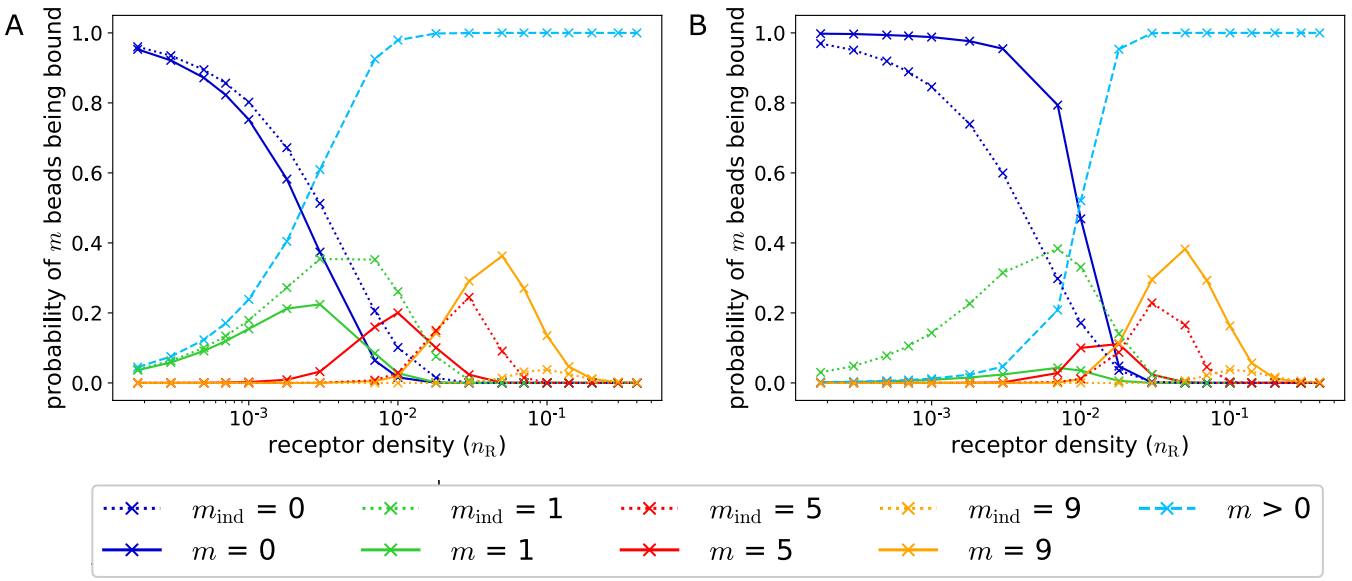

FIG. S8: Probability of m beads being bound in a system of parameters $l = 5$ and $f = 2kT$. The dashed lines are for ten monovalent clients and the solid lines are for a single decavalent client. These plots are for systems (A) without crowders, (B) with crowders at density $d = 0.4$.

to directional binding. Isotropic binding also reduces the competition for binding to a given receptor as multiple client beads can bind to the same receptor, unlike in the directional binding case.

Overall, the earlier onset of cooperativity strengthens superselective effect where crowders are present. This can be observed by comparing the magnitude of the peaks in Fig. S7 and Fig. 4 of the main text. However, this change in cooperativity is not sufficient to introduce superselective binding in the case where crowders are absent. We also emphasize that the possibility for a client to form multiple bonds with a receptor bead differentiate the isotropic binding case from the directional binding scenario. These two cases cannot be mapped onto each other through a simple rescaling of the interaction energies. Nevertheless, the trends in superselective behavior with respect to crowder density are analogous for the two binding models, demonstrating that the introduction or enhancement of superselectivity by crowders does not depend on the details of the bonding.

* halim.kusumaatmaja@durham.ac.uk
† m.a.miller@durham.ac.uk

[1] D. S. Protter, B. S. Rao, B. Van Treeck, Y. Lin, L. Mizoue, M. K. Rosen, and R. Parker, Cell Rep. **22**, 1401 (2018).
[2] D. Frenkel and B. Smit, *Understanding Molecular Simulation* (Academic Press, 2001) p. 29.
[3] F. J. Martinez-Veracoechea and D. Frenkel, Proc. Nat. Acad. Sci. USA **108**, 10963 (2011).
[4] T. S. Harmon, A. S. Holehouse, M. K. Rosen, and R. V. Pappu, eLife **6**, e30294 (2017).
[5] S. F. Banani, A. M. Rice, W. B. Peeples, Y. Lin, S. Jain, R. Parker, and M. K. Rosen, Cell **166**, 651 (2016).
[6] Y. Jo and Y. Jung, Chem. Sci. **11**, 1269 (2020).
[7] S. Kroschwald, S. Maharana, D. Mateju, L. Malinovska, E. Nüske, I. Poser, D. Richter, and S. Alberti, eLife **4**, e06807 (2015).
[8] W. Xing, D. Muhlrad, R. Parker, and M. K. Rosen, eLife **9**, e56525 (2020).
[9] K. K. Nakashima, M. A. Vibhute, and E. Spruijt, Frontiers in Molecular Biosciences **6**, 21 (2019).